



# Role of solution structure in the electrochemical intercalation of $\text{Ca}^{2+}$ into graphite layers

Yuichiro Nishimura<sup>1</sup> · Naoki Nakatani<sup>1</sup> · Kiyoharu Nakagawa<sup>1,2</sup>

Received: 12 January 2021 / Revised: 19 July 2021 / Accepted: 9 August 2021 / Published online: 26 August 2021  
© The Author(s), under exclusive licence to Springer-Verlag GmbH Germany, part of Springer Nature 2021

## Abstract

In this study, we investigated the electrochemical intercalation of  $\text{Ca}^{2+}$  into graphite as an anode material for calcium-ion batteries (CIBs). The electrochemical intercalation of  $\text{Ca}^{2+}$  into a graphite electrode is possible when  $\gamma$ -butyrolactone (GBL) is utilized as a solvent, resulting in a reversible charge/discharge capacity. The GBL-based electrolyte allows a reversible redox reaction, thereby resulting in the intercalation and deintercalation of  $\text{Ca}^{2+}$  within the graphite electrode. Conversely,  $\text{Ca}^{2+}$  cannot be intercalated between the graphite layers in the ethylene carbonate–diethyl carbonate (EC–DEC)–based electrolyte. Analyses of the solution structures of both cases indicated that the interaction between the GBL solvent and  $\text{Ca}^{2+}$  was weak whereas that between the EC–DEC solvent and  $\text{Ca}^{2+}$  was strong. As a result of analyzing the surface of the negative electrode after charging and discharging from XPS, it was confirmed that a component that seems to be a solid electrolyte interphase (SEI) was confirmed in the graphite electrode using the GBL-based electrolyte.

**Keywords** Calcium-ion battery · Electrochemical intercalation · Solution structure · Graphite anode

## Introduction

Secondary batteries utilizing divalent cations ( $\text{Mg}^{2+}$  and  $\text{Ca}^{2+}$ ) instead of  $\text{Li}^+$  as charge carriers are attracting attention in the development of post–lithium-ion batteries (LIBs) [1–5]. Utilizing divalent cations, it is possible to obtain twice the capacity of LIBs. Among these divalent cations,  $\text{Ca}^{2+}$  demonstrates unique advantages [6, 7]. Compared to  $\text{Mg}^{2+}$ , the standard electrode potential of  $\text{Ca}^{2+}$  is approximately 0.5 V lower (–2.87, –2.37 V vs. SHE for Ca, Mg), and it can utilize a high operating voltage [1]. Additionally, since calcium is the fifth most abundant element, it is advantageous, in terms of sustainability [8]. Because of these features, calcium-ion batteries (CIBs) exhibit great potential as alternatives to LIBs. However, there are some limitations to the development of CIBs regarding the electrode materials and electrolytes [9, 10]: a Ca metal electrode

prevents the reversible dissolution/precipitation of  $\text{Ca}^{2+}$  in conventional organic electrolytes because of the surface film that is formed on the Ca metal [9, 11]. Furthermore, since divalent cations, such as  $\text{Ca}^{2+}$ , exhibit stronger Lewis acidity than  $\text{Li}^+$ , they can form strong solvation structures with solvent molecules in the electrolyte and possess high desolvation energy [9, 12]. Thus, the optimization of a  $\text{Ca}^{2+}$  host material and the design of an electrolytic solution to address these limitations are desired.

Graphite is widely employed as a negative electrode material for general LIBs because of its inexpensiveness, safety, and capacity [13]. In LIBs,  $\text{Li}^+$  is stored in the graphite layers to form a Li–graphite intercalation compound (Li–GIC) [14], although the intercalation of  $\text{Ca}^{2+}$  into graphite layers was previously limited to reports by chemical methods [15–17]. Recently, however, it was reported that the electrochemical intercalation of  $\text{Ca}^{2+}$  into graphite was possible [18, 19]. These reports indicated that graphite could be employed as a negative electrode material for CIBs and that a charge/discharge system like in LIBs could be constructed.

The electrolyte of LIBs is designed to favor the positive and negative electrode materials considering the charge and discharge capacity, the composition of the solid electrolyte interphase (SEI), and the rate characteristics [20–23]. To charge and discharge LIBs, it is necessary to form an SEI on

✉ Kiyoharu Nakagawa  
kiyoharu@kansai-u.ac.jp

<sup>1</sup> Graduate School of Science and Engineering, Kansai University, Suita, Osaka 564-8680, Japan

<sup>2</sup> Department of Chemical, Energy and Environmental Engineering and High Technology Research Core (HRC), Kansai University, Suita, Osaka 564-8680, Japan

the surface of the graphite electrode during the first cycle. Therefore, a solvent containing ethylene carbonate (EC) is utilized as the solvent for the electrolyte of LIBs. However, since EC exhibits both a narrow liquid temperature range and high viscosity, it is not an ideal solvent. Conversely,  $\gamma$ -butyrolactone (GBL) demonstrates advantageous physical properties, such as a wide liquid temperature range and low viscosity. Among them, we focused on the solution structure of the electrolytes using these two types of solvents. There are few studies focusing on the solution structure in the intercalation of  $\text{Ca}^{2+}$  between graphite layers.

In this study, the electrochemical intercalation of  $\text{Ca}^{2+}$  into a graphite electrode was conducted employing both EC–DEC- and GBL-based electrolytes containing calcium salt  $\text{Ca}(\text{ClO}_4)_2$ . Thereafter, the effect of the organic solvent on the electrochemical properties of the graphite electrode was analyzed in terms of the solution structure.

## Experimental

Spherical natural graphite (CGB-10, Nippon Graphite Industries, Ltd.) was used as a working electrode and an activated carbon fiber cloth (Kynol, Gun-ei Chemical Industry, Ltd.) was used as a counter electrode. Cellulose fiber (ADVANTEC Toyo, Ltd.) was used as the separator. The electrolytic solution was prepared by dissolving (1 M  $\text{Ca}(\text{ClO}_4)_2$ ) in EC:diethyl carbonate (DEC) = (1:1 by volume) and  $\gamma$ -butyrolactone (GBL). These chemicals were purchased from FUJIFILM Wako Pure Chemical Ltd.

To analyze the electrochemical behavior of the graphite electrode in the organic electrolytes, cyclic voltammetry (CV) and charge/discharge measurements were conducted. The CV measurements were conducted at a scanning potential of 0–3.5 V and a scan rate of 1 mV s<sup>-1</sup>, and the charge/discharge measurements were conducted at a scanning potential of 0–3.5 V and a current density of 15.38 mA g<sup>-1</sup>.

Laser Raman spectroscopy (NRS-3100, JASCO) was employed to analyze the graphite intercalation compounds and electrolytes. The wavelength of the exciting laser light source was 532 nm, and the laser power was 100 mW. The measurement was conducted with an exposure time of 5 s and consisted of eight integrations. The wavenumber of the Raman shift was calibrated utilizing Si and polypropylene standards. The analysis of the graphite intercalation compounds was conducted after 3 cycles of charging and discharging. The first cycle was considered to involve the formation of a film by reductive decomposition, so it was not representative of subsequent cycles.

X-ray diffractometry (XRD, SmartLab, Rigaku) was employed to calculate the interlayer distance before and after

charging from the peak position on the (002) plane according to Eq. (1):

$$d = \frac{\lambda}{2\sin\theta_C} \quad (1)$$

where  $d$  is the phase-spacing,  $\lambda$  is the (Cu-K $\alpha$ ) X-ray wavelength, and  $\theta_C$  is the diffraction angle of graphite. The number of stages was calculated from Eqs. (2), (3), and (4) [9, 24]:

$$d_{00l} = \frac{I_c}{l} \text{ and } d_{00l+1} = \frac{I_c}{l+1} \quad (2)$$

$$l = \frac{1}{\left(\frac{\sin\theta_{00l+1}}{\sin\theta_{00l}} - 1\right)} \quad (3)$$

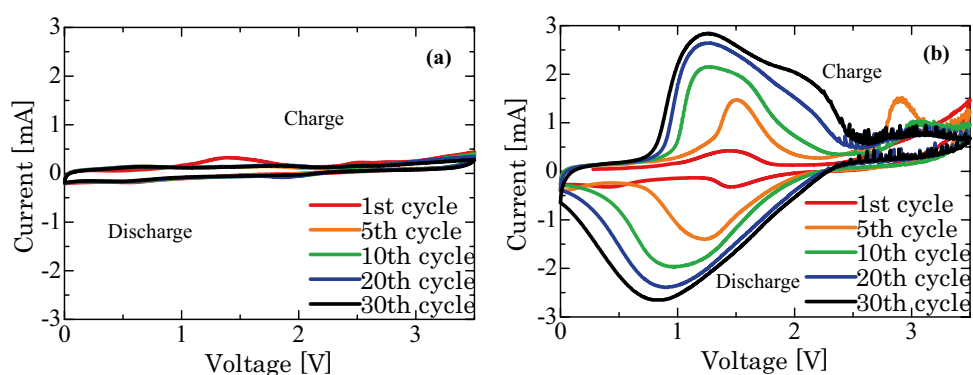
$$I_C = d_i + (n - 1) \times d_{host} \quad (4)$$

where  $d_{00l}$  and  $d_{00l+1}$  are the d-spacing values of the (00  $l$ ) and (00  $l+1$ ) planes, respectively. Here,  $I_C$  is the repeat-period distance,  $d_i$  is the intercalation-layer spacing,  $d_{host}$  is the graphite spacing, and  $n$  is the number of stages. The X-ray wavelength was 0.15406 nm, the voltage was 45 kV, and the current was 200 mA. Divergence slit (DS) was 1/2°, receiving slit (RS) was 0.15 nm, and scattering slit (SS) was 1/2°. The range of the measurement was 5–90°, and the scan speed was 50° min<sup>-1</sup>. The measurement was conducted after 3 cycles of charging and discharging to obtain representative results.

Fourier transform infrared (FT-IR; FT/IR-4200, JASCO) spectroscopy was employed to analyze the solution structure and the components of the graphite electrode surface after discharging. The measurement range was 500–4000 cm<sup>-1</sup> at a resolution of 4 cm<sup>-1</sup> and the integration number was 400 times. The solution structure was measured by the liquid-film method utilizing BaF<sub>2</sub> as the window board and spacer with a thickness of 0.012 mm whereas the components of the graphite electrode surface were measured by the KBr tablet method.

The surface morphologies of the graphite electrode before charging and after discharging were observed using X-ray photoelectron spectroscopy (XPS; PS-9000MX, Nihon Denshi) that was employed for the analysis of the components of the graphite electrode surface after discharging. Peak separation was performed on the C 1s spectrum, and the abundance ratio was calculated from the area ratio. The X-ray source was Mg-K $\alpha$  (average energy = 1253.56 eV), the voltage was 10 kV, and the current was 10 mA. The measurement was conducted at an exposure time of 10 s and an integration number of 16 times.

**Fig. 1** Cyclic voltammograms of the graphite electrode in (a) 1 M  $\text{Ca}(\text{ClO}_4)_2/\text{EC-DEC}$  and (b) 1 M  $\text{Ca}(\text{ClO}_4)_2/\text{GBL}$ , both at a scan rate of 1 mV/s



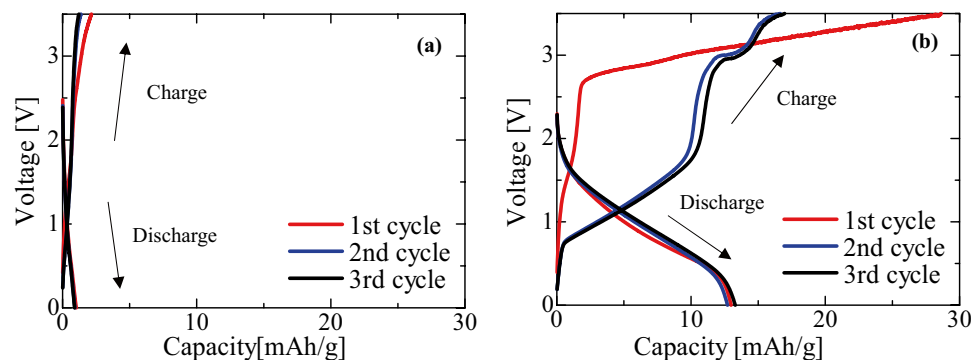
## Results and discussion

Figure 1 shows cyclic voltammograms of the graphite electrodes in both EC–DEC- and GBL-based electrolytes. In the EC–DEC-based electrolyte (Fig. 1a), the graphite electrode did not indicate a reversible redox reaction; only ion adsorption and desorption were observed. Conversely, in the GBL-based electrolyte (Fig. 1b), a reduction reaction was observed during the charging process in the vicinity of 1.0–2.0 V, and an oxidation reaction was observed during the discharging process in the vicinity of 0.5–2.0 V. These reactions were caused by the intercalation and deintercalation reactions of  $\text{Ca}^{2+}$  into the graphite layers within the electrode. As the cycle was repeated, the peak value of the current increased, and the potential range where the reaction occurred also increased. Therefore, the intercalation and deintercalation reactions may have progressed further. Generally, in LIBs, the current value of the reduction reaction due to the intercalation of  $\text{Li}^+$  is larger than that of the oxidation reaction due to its deintercalation. However, in the case of  $\text{Ca}^{2+}$ , the current value of the oxidation reaction was larger than that of the reduction reaction (Fig. 1b). Since the current value of the cyclic voltammogram represents the reaction rate, it was evidently challenging for  $\text{Ca}^{2+}$  to intercalate into the graphite layers, although  $\text{Ca}^{2+}$  in the graphite layers was readily deintercalated.

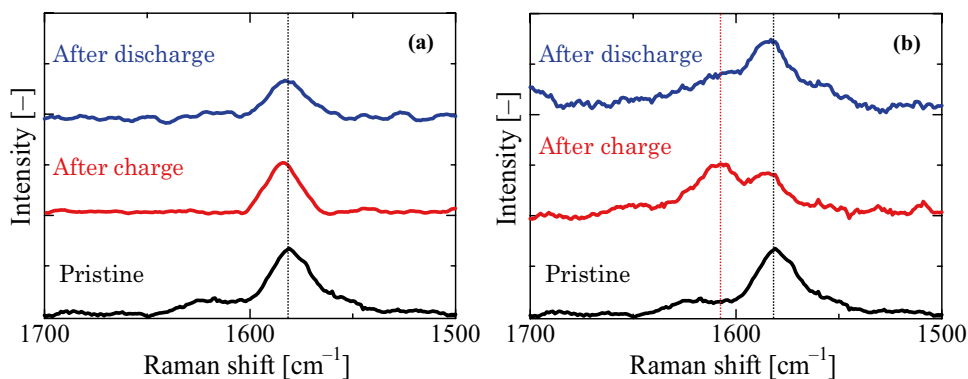
Figure 2 shows the charge/discharge profiles of the graphite electrode in both EC–DEC- and GBL-based electrolytes. In this study, charge is defined as reduction or  $\text{Ca}^{2+}$  intercalation, and discharge is defined as oxidation,  $\text{Ca}^{2+}$  deintercalation [18]. In the EC–DEC-based electrolyte, no plateau section was found, and little volume capacity was obtained. Moreover, in the GBL-based electrolyte, the charge/discharge action exhibited an irreversible capacity in the first cycle. SEI may have been formed on the surface of the graphite electrode by reductive decomposition of the GBL-based electrolyte. From the second cycle onward, the potential plateaued from about 0.7 to 1.8 V. This suggests that  $\text{Ca}^{2+}$  had been intercalated between the graphite layers. The charge capacity after 3 cycles was  $17.0 \text{ mAh g}^{-1}$ , which is approximately 14 times larger than was obtained with the EC–DEC-based electrolyte. In the GBL-based electrolyte, the discharge capacity increases slightly, which is thought to be due to surface adsorption by the electric double layer of ions [25]. Additionally, there was a correlation between the potential of the charge/discharge curve and the peak position of the cyclic voltammogram. In this study, however, the electrochemical measurements were performed utilizing a two-electrode cell. Detailed studies of the intercalation and deintercalation voltages of  $\text{Ca}^{2+}$  employing a three-electrode cell are ongoing.

Raman spectroscopy was employed to determine whether Ca-GIC was formed after the charging process (Fig. 3). In

**Fig. 2** Charge/discharge curves of the graphite electrode in (a) 1 M  $\text{Ca}(\text{ClO}_4)_2/\text{EC-DEC}$  and (b) 1 M  $\text{Ca}(\text{ClO}_4)_2/\text{GBL}$



**Fig. 3** Raman spectrum of the graphite electrode after 3 cycles of charging and discharging in (a) 1 M  $\text{Ca}(\text{ClO}_4)_2/\text{EC-DEC}$  and (b) 1 M  $\text{Ca}(\text{ClO}_4)_2/\text{GBL}$



the EC-DEC-based electrolyte, a reversible redox reaction was not observed in the CV measurements. Therefore, the stage of the graphite electrode after the charging process was similar to that before charging (Fig. 3a). This demonstrated that  $\text{Ca}^{2+}$  could not be intercalated into the graphite layers by utilizing the EC-DEC solvent generally employed in LIBs. However, the Raman spectrum of the graphite electrode after the charging process in the GBL-based electrolyte displayed a new peak in the vicinity of  $1610\text{ cm}^{-1}$ , in addition to the  $I_G$  band derived from the graphite structure (Fig. 3b). Since the peak around  $1610\text{ cm}^{-1}$  was derived from the graphite intercalation compound [26, 27], we interpreted this to mean that  $\text{Ca}^{2+}$  had been successfully intercalated into the graphite layers. Moreover, the Raman spectrum of the graphite electrode after the discharging process in the GBL-based electrolyte was the same as the state before charging. This also supports the conclusion that  $\text{Ca}^{2+}$  had been electrochemically intercalated/deintercalated between the graphite layers in the GBL-based electrolyte. These findings confirm that electrochemical intercalation/deintercalation of  $\text{Ca}^{2+}$  into graphite was successful without a special treatment of the graphite, as obtained in LIBs. Furthermore, the reversible redox reaction, observed in the CV measurements, was due to the intercalation/deintercalation reaction of  $\text{Ca}^{2+}$  into the graphite layers.

Similarly, XRD was employed to evaluate the intercalation/deintercalation of  $\text{Ca}^{2+}$  between the graphite layers

(Fig. 4). Before charging, the XRD pattern of the graphite electrode displayed a sharp peak from the (002) plane of graphite at  $26.5^\circ$ , and the interlayer distance ( $d_{002}$ ) was  $0.335\text{ nm}$ . In the EC-DEC-based electrolyte, the  $26.5^\circ$  peak derived from the (002) plane did not shift after charging/discharging, thus indicating that  $\text{Ca}^{2+}$  intercalation into the graphite layers did not proceed (Fig. 4a). Conversely, in the GBL-based electrolyte, the peak due to the (002) plane shifted to  $24.0^\circ$  after charging, thereby confirming that the interlayer distance had expanded from  $0.335$  to  $0.358\text{ nm}$  (Fig. 4b). After discharging, the peak returned to the original peak position of the (002) plane, indicating that reversible intercalation/deintercalation of  $\text{Ca}^{2+}$  was possible in the graphite electrode. Here, the values of  $2\theta_{00l}$  and  $2\theta_{00l+1}$  were  $24.81^\circ$  and  $29.13^\circ$  ( $d_{00l} = 0.358\text{ nm}$  and  $d_{00l+1} = 0.306\text{ nm}$ ), respectively. According to Eqs. (2) and (3), the calculated values of  $l$  and  $l_c$  were about 6 and  $2.148\text{ nm}$ , respectively. Therefore, from Eq. (4), we estimate that the negative electrode material approximately possessed a stage 6 structure after charging. Furthermore, in the GBL-based electrolyte, the peak returning to the (002) plane after the discharging process became broad. However, the ratio,  $I_G/I_D$ , of the intensities of the G-band (the peaks at  $1580\text{ cm}^{-1}$ ) and D-band (the peaks at  $1350\text{ cm}^{-1}$ ) calculated from the Raman spectrum was 3.38 and 3.26 before charging and after discharging, respectively. Since the  $I_G/I_D$  ratio remained generally unchanged, we conclude that the crystallinity of

**Fig. 4** XRD spectrum of the graphite electrode after 3 cycles of charging and discharging in (a) 1 M  $\text{Ca}(\text{ClO}_4)_2/\text{EC-DEC}$  and (b) 1 M  $\text{Ca}(\text{ClO}_4)_2/\text{GBL}$

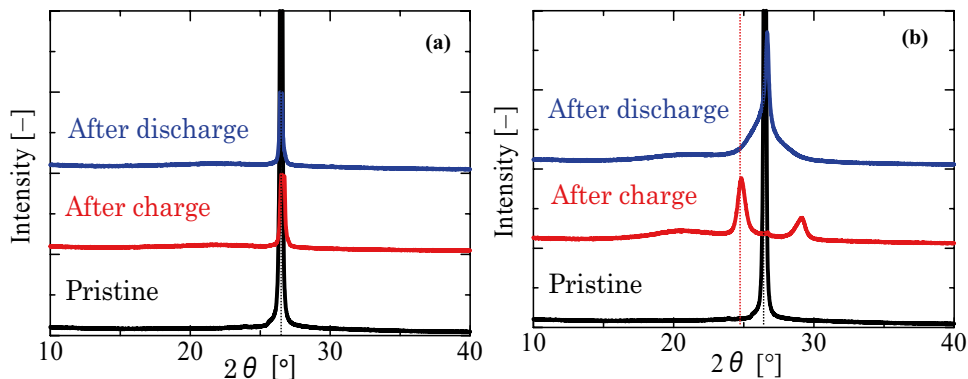
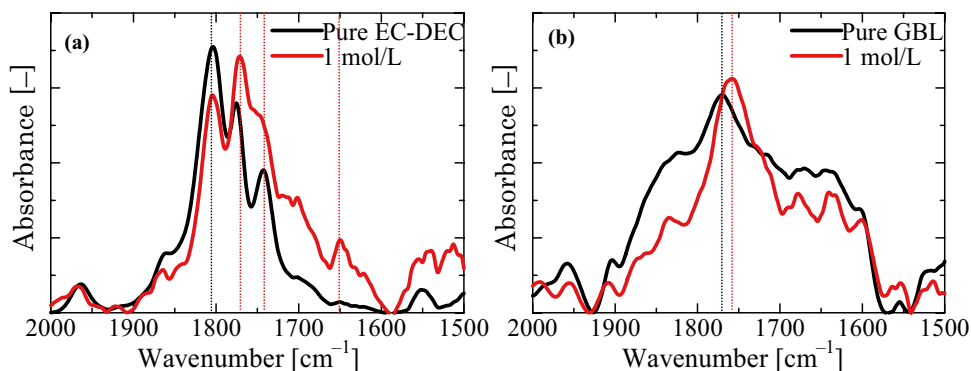


**Fig. 5** FT-IR spectrum for the stretching vibration band of C=O double bonds in (a) 1 M  $\text{Ca}(\text{ClO}_4)_2/\text{EC-DEC}$  and (b) 1 M  $\text{Ca}(\text{ClO}_4)_2/\text{GBL}$



the graphite electrode was maintained before charging and after discharging.

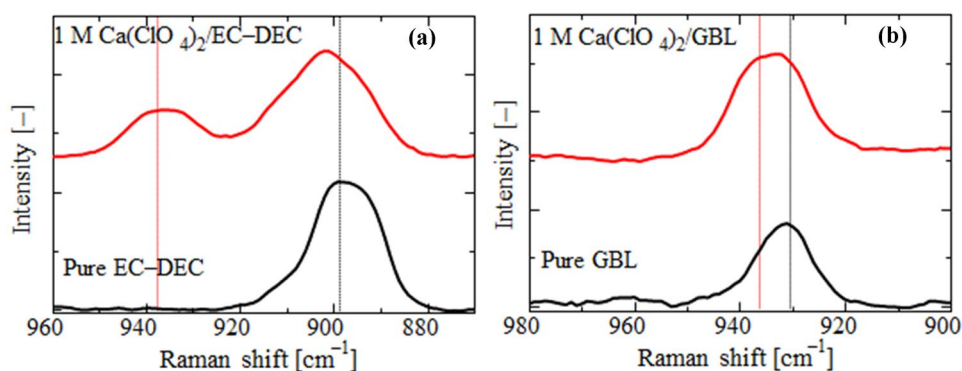
Figure 5 shows the FT-IR spectrum of the C=O stretching vibration in the EC-DEC- and GBL-based electrolytes containing  $\text{Ca}(\text{ClO}_4)_2$ . From Fig. 5a, the EC solvent exhibited peaks at 1800 and 1775  $\text{cm}^{-1}$ , while DEC exhibited a peak at 1740  $\text{cm}^{-1}$  because of the C=O double bond. By dissolving the electrolyte in the EC-DEC mixed solvents, the peak at 1800  $\text{cm}^{-1}$  decreased and that at 1775  $\text{cm}^{-1}$  increased. Furthermore, the peak at 1740  $\text{cm}^{-1}$  became broad, and a new peak at 1650  $\text{cm}^{-1}$  was confirmed in that vicinity. We assume that this was caused by the change in the molecular vibration due to the coordination of the solvent molecules with  $\text{Ca}^{2+}$ . Contrary to the peak around 1750  $\text{cm}^{-1}$  in the GBL solvent, there was essentially no change, even when the electrolyte was dissolved (Fig. 5b). Therefore, the GBL solvent was largely unaffected by the electrostatic effect of  $\text{Ca}^{2+}$ , and interactions between the ion and solvent molecules were smaller than for the EC-DEC solvent.

Figure 6 shows the Raman spectrum of the C–O stretching vibration in EC-DEC- and GBL-based electrolytes containing  $\text{Ca}(\text{ClO}_4)_2$ . The EC and DEC peaks appeared in the spectrum at approximately 895 and 900  $\text{cm}^{-1}$ , respectively. As seen in Fig. 6a, the EC-DEC mixed solvent appeared in the spectrum at around 900  $\text{cm}^{-1}$ . When  $\text{Ca}(\text{ClO}_4)_2$  was dissolved, a new band was confirmed around 940  $\text{cm}^{-1}$

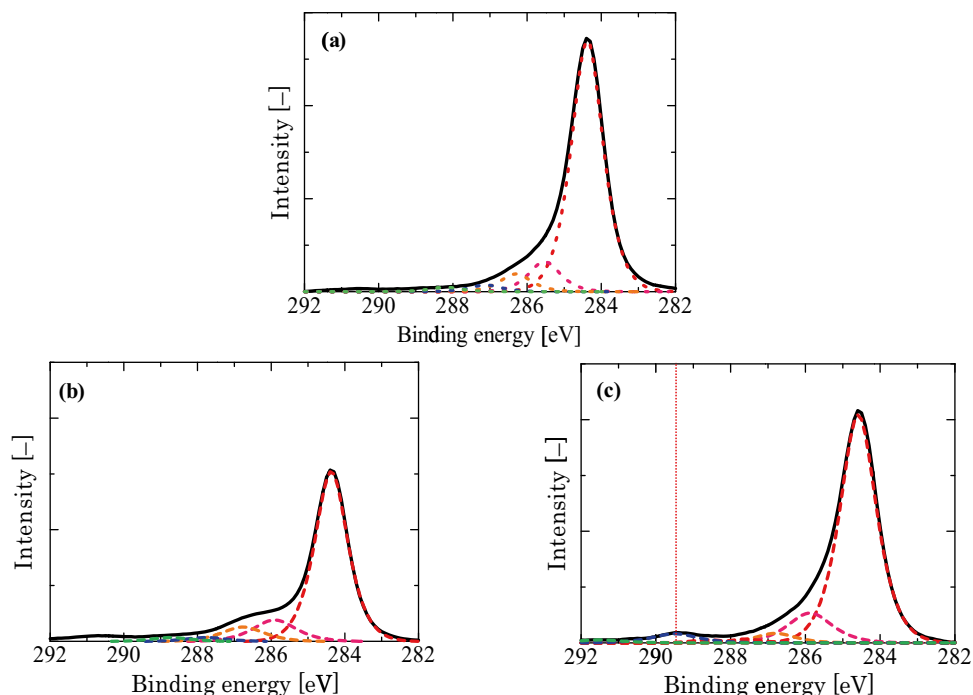
(Fig. 6(a)). This band was derived from a solvent molecule that was coordinated to  $\text{Ca}^{2+}$  to form a solvated ion. When Li salt was dissolved in the EC-based electrolyte, the width of the band shift was approximately 10  $\text{cm}^{-1}$  whereas the Ca salt produced about a 40  $\text{cm}^{-1}$  shift in the width [28]. Since this shift in the width of the band represents the strength of the interaction between the ion and solvent molecules [29], we conclude that a very strong interaction existed between  $\text{Ca}^{2+}$  and the EC-DEC solvent.  $\text{Ca}^{2+}$  could not be intercalated between the graphite layers in the EC-DEC-based electrolyte probably because  $\text{Ca}^{2+}$  could not be desolvated from solvated  $\text{Ca}^{2+}$ . Conversely, the GBL solvent induced a band around 930  $\text{cm}^{-1}$ . No new bands were observed, even when a Ca salt was dissolved, and the bandwidth displayed only about 3  $\text{cm}^{-1}$  spreading (Fig. 6b), indicating that the interaction between  $\text{Ca}^{2+}$  and the GBL solvent was very weak.

These results correspond to those of FT-IR. Therefore, the order of the strength of the interaction with  $\text{Ca}^{2+}$  is  $\text{GBL} < \text{EC-DEC}$ . This order agrees with the order of the dielectric constants of those solvents (GBL: 39.1 and EC: 89.8 (EC-DEC is focused on EC)), and the larger the value of the dielectric constant, the readier the solvation proceeded. Therefore, we assumed that the stability achieved when  $\text{Ca}(\text{ClO}_4)_2$  was dissociated to become solvated  $\text{Ca}^{2+}$  also conformed to this order. Thus, the desolvation of solvated  $\text{Ca}^{2+}$  on the surface of graphite was greatly eased in the case of the GBL-based electrolyte, resulting in

**Fig. 6** Raman spectrum for the symmetric stretching vibration band of the C–O single bonds in (a) 1 M  $\text{Ca}(\text{ClO}_4)_2/\text{EC-DEC}$  and (b) 1 M  $\text{Ca}(\text{ClO}_4)_2/\text{GBL}$



**Fig. 7** C 1 s XPS spectrum of the graphite electrode: (a) pristine and after discharging in (b) 1 M  $\text{Ca}(\text{ClO}_4)_2/\text{EC-DEC}$  and (c) 1 M  $\text{Ca}(\text{ClO}_4)_2/\text{GBL}$



the successful intercalation of  $\text{Ca}^{2+}$  between the graphite layers.

The XPS results for the C 1 s spectrum are shown in Fig. 7. In the EC–DEC-based electrolyte, only the peaks derived from C–C ( $\text{sp}^2$ ) and oxygen-containing functional groups were confirmed in the graphite electrode after discharging (Fig. 7b). Conversely, the graphite electrodes that were charged/discharged in the GBL-based electrolyte were newly confirmed to display peaks at approximately 289.5 eV compared to before charging/discharging (pristine) (Fig. 7c). Furthermore, the FT-IR analysis was performed with a GBL-based electrolyte in which the precipitates were confirmed from the XPS results. As seen in Fig. 8, the peaks at  $2920\text{--}2850\text{ cm}^{-1}$ ,  $1750\text{--}1700\text{ cm}^{-1}$ , and  $1150\text{--}1090\text{ cm}^{-1}$  correspond to the

C–H stretching vibrations, C=O asymmetric stretching vibrations, and C–O stretching vibrations, respectively. Remarkable carboxylate peaks were also confirmed at  $1540\text{ cm}^{-1}$  and  $1457\text{ cm}^{-1}$ , and Aurbach et al. reported that such carboxylate peaks are typical of the derivatives of butyric and  $\beta$ -hydroxy butyric acids [10]. Furthermore, we obtained similar IR spectrum at positions similar to the results of Aurbach et al. [10, 30], and we therefore conclude that the same precipitates may have been deposited on the surface of the graphite electrode. Therefore, in the GBL-based electrolyte, byproducts formed during the desolvation reaction were confirmed, and indicating that  $\text{Ca}^{2+}$  had been intercalated between the graphite layers. In this case, it was necessary to investigate further the presence or absence of the possibility of co-intercalation with GBL to clarify the progress of the desolvation reaction.

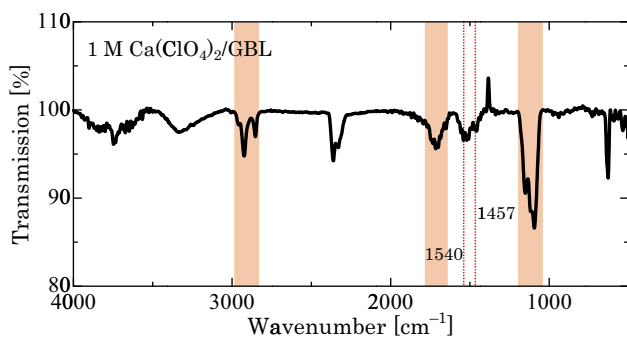


**Fig. 8** FT-IR spectrum of the graphite electrode after discharging in 1 M  $\text{Ca}(\text{ClO}_4)_2/\text{GBL}$

## Conclusions

In the GBL-based electrolyte, a reversible redox reaction was observed. Raman spectroscopy indicated that the reversible redox reaction was due to the intercalation/deintercalation of  $\text{Ca}^{2+}$  into the graphite layers. Conversely, in the EC–DEC-based electrolyte, the graphite electrode did not demonstrate a reversible redox reaction, indicating that  $\text{Ca}^{2+}$  had not been intercalated into the graphite layers. The solution structure of each electrolyte was analyzed using Raman spectroscopy and FT-IR, which confirmed that the GBL-based electrolyte was more likely to be desolvated than the

EC–DEC-based electrolyte. Such a solution structure was presumed to be formed because GBL has a lower dielectric constant than EC. Thus, the difference in the solution structure of the organic electrolyte greatly influenced the potential for intercalation of  $\text{Ca}^{2+}$  between the graphite layers.

**Acknowledgements** The authors are grateful to Nippon Graphite Industries, Ltd., for supplying us with spherical natural graphite for our research. The authors would like to thank Enago ([www.enago.jp](http://www.enago.jp)) for the English language review.

**Funding** This work was supported by JSPS KAKENHI Grant Number JP20K12274.

## References

- Muldoon J, Bucur CB, Gregory T (2014) *Chem Rev* 114:11683
- Lipson AL, Pan B, Lapidua SH, Liao C, Vaughey J, Ingram BJ (2015) *Chem Mater* 27:8442
- Tojo T, Sugiura Y, Inada R, Sakurai Y (2016) *Electrochem Acta* 207:22
- Siegal MP, Yelton WG, Perdue BR, Sava Gallis DF, Schwarz H (2016) *J Electrochem Soc* 163:A1030
- Placke T, Kloepsch R, Dühnen S, Winter M (2017) *J Solid State Electrochem* 21:1939–1964
- Ponrouch A, Tchitchekova D, Frontera C, Barde F, Arroyo-de Dompablo ME, Palacin MR (2016) *Electrochem Commun* 66:75–78
- Lee C, Jeong YT, Nogales PM, Song HY, Kim YS, Yin RZ, Jeong SK (2019) *Electrochem Commun* 98:115–118
- Alekseenko V, Alekseenko A (2014) *J Geochem Explor* 147:245
- Park J, Xu ZL, Yoon G, Park SK, Wang J, Hyun H, Park H, Lim J, Ko YJ, Yun YS, Kang K (2020) *Adv Mater* 32:1904411
- Aurbach D, Skaletsky R, Gofar Y (1991) *Electrochem Soc* 138:3536–3545
- Ponrouch A, Frontera C, Bardé F, Palacín M (2016) *Nat Mater* 15:169
- Forero-Saboya JD, Marchante E, Atrajjo RB, Monti D, Johansson P, Ponrouch A (2019) *J Phys Chem* 123:29524–29532
- Fukuda K, Umeno T, Hara Y (2004) *Material Integration* 17:45–50
- Ogumi Z, Inaba M (1998) *Bull Chem Soc* 71:521–534
- Herold C, Emery N, Mareche JF, Lagrange P (2008) *TANSO* 223:166–173
- Sugawara K, Sato T, Takahashi T (2009) *Nat Phys* 5:40–43
- Yang SL, Sobota JA, Howard CA, Pickard CJ, Hashimoto M, Lu DH, Mo SK, Kirchmann PS, Shen ZX (2014) *Nat Commun* 5:1–5
- Richard Prabakar SJ, Ikhe AB, Park WB, Chung KC, Park H, Kim KJ, Ahn D, Kwak JS, Sohn KS, Pyo M (2019) *Adv Sci* 6:1902129
- Wu S, Zhang F, Tang YB (2018) *Adv Sci* 5:1701082
- Jeong SK, Inaba M, Iriyama Y, Abe T, Ogumi Z (2003) *Electrochem Soild-State Lett* 6:A13
- Xu K (2004) *Chem Rev* 104:4303
- Seo DM, Reininger S, Kutcher M, Redmond K, Euler WB, Lucht BL (2015) *J Phys Chem* 119:14038
- Nakatani N, Kishida K, Nakagawa K (2018) *J Electrochem Soc* 165(9):A1621
- Watanabe N, Matsuo K, Touhara H, Horita K, Mizutani Y, Ohashi K, Takahashi Y, Akuzawa N, Fujii R, Dohi T (1986) Graphite intercalation compound. Kindai-Hensyusya Inc, Tokyo
- Wang C, Sawicki M, Emani S, Liu C, Shaw LL (2015) *Electrochem Acta* 161:322–328
- Inaba M, Yoshida H, Ogumi Z, Abe T, Mizutani Y, Asano M (1995) *J Electrochem Soc* 142:20
- Sole C, Drewett NE, Hardwick LJ (2014) *Faraday Discuss* 172:223
- Morita M, Asai Y, Yoshimoto N, Ishikawa M (1998) *J Chem Soc Faraday Trans* 94:3451
- Yamaguchi T, Kimura Y, Hirota N (1998) *J Chem Phys* 109:9084
- Aurbach D (1989) *J Electrochem Soc* 136:906–913

**Publisher's Note** Springer Nature remains neutral with regard to jurisdictional claims in published maps and institutional affiliations.